Int. Journ. of Laser Science, Vol. 1, pp. 17–29
Reprints available directly from the publisher.
Photocopying permitted by license only.

Colour Fusion Polarization Ghost Imaging

X. YANG, Y. ZHANG, C. YANG, L. XU, Q. WANG AND Y. ZHAO*

Department of Physics, Harbin Institute of Technology, Harbin 15000, Heilongjiang Province, China

In conventional two-dimensional (2-D) ghost imaging (GI), intensity images can be obtained by utilizing the intensity correlation between signals in the reference path and test path. Grey values in ghost imaging represent the transmission coefficient or reflection coefficient of the target. In this study, colour fusion polarization ghost imaging (CPGI) system is proposed to acquire polarization image of target through Stokes parameters. A polarized chromatic value (PCV) is introduced in this system to describe Stokes parameters in a pseudo-colour way. Target information can easily be extracted from the result of CPGI system. The proposed method can be employed successfully to identify targets, promoting wider application of ghost imaging systems.

Keywords: Laser, ghost imaging (GI), colour fusion polarization image system (CPGI), Stokes parameter, polarized chromatic value (PCV)

1 INTRODUCTION

Conventional two-dimensional (2-D) thermal ghost imaging (GI) can obtain intensity images of targets using the intensity correlation of the light beams in the reference path and test path [1–5]. Grey values of the intensity images represent the transmission coefficient or reflection coefficient of the target. Computational ghost imaging (CGI) [6–8] and compressive sensing ghost imaging (CSGI) [9–11] are popular methods, favoured for their high-quality imaging properties and rapid imaging speed.

Due to the distinct advantages of the ghost imaging, many researchers have attempted to broaden its application field [12–17]. Previous studies typically focus on intensity images, in which grey values relate to the reflection coefficient (or the transmission coefficient) of the target. When there are two targets

*Corresponding author: Tel: +86 (0)451 8641 4120; E-mail: zhaoyuan@hit.edu.cn

with the same reflection coefficient (or the same transmission coefficient) in the field of view, the two targets can-not be distinguished through intensity images; hence, polarization ghost imaging (PGI), which measures degree of polarization (DOP) distribution of reflected light from target, is proposed to solve this problem [18–20].

In the field of polarization imaging, Stokes parameters contain more polarization information than DOP. Hence, it is better to distinguish targets with same reflection coefficient through Stokes parameters distribution image than that of DOP. In this study, we propose a colour-fusion polarization ghost imaging (CPGI) system to measure Stokes parameters distribution reflected from target. Computational experiment is also performed in this study, and the results indicate that CPGI can distinguish the different targets with same reflection coefficient (or the same transmission) much better than PGI and GI system.

2 SYSTEM DESCRIPTION AND THEORETICAL ANALYSIS

The CPGI system is shown in Figure 1. The experiment setup is based on the CGI experiment setup. A spatial light modulator (SLM) is used to modulate the laser and generate the pseudorandom speckle pattern. The system selects a reflecting target similar theoretically to a transmission target. Unlike the

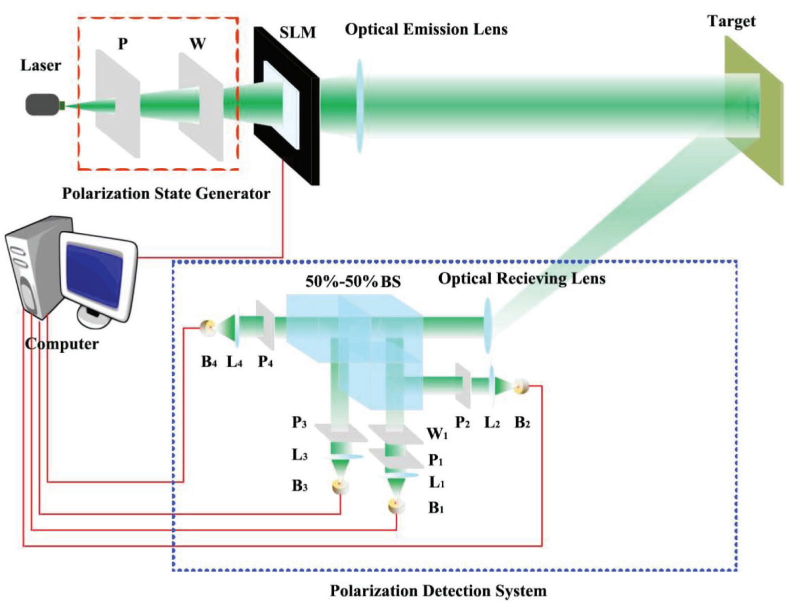

FIGURE 1
Schematic diagram of the polarization ghost imaging system.

CGI set up, the proposed system features a polarization state generator between the SLM and laser source. The polarization state generator comprises of a linear polarizer (LP) *P* and a quarter-wave plate (QWP) *W*.

After being modulated by the polarization state generator and the SLM, the light is emitted to illuminate the target. All parts of the target share the same reflectivity. The polarization detection system (marked by the blue dotted lines in Figure 1) measures light reflected from the target. Three 50%-50% non-polarization beam splitters (BS) in the polarization detection system separate the echoed light into four test arms. Four convex lenses L_1, L_2, L_3 and L_4 are placed in the four test arms to converge the light on four same type detectors B_1, B_2, B_3 and B_4, respectively. The detectors are independent of each other.

Test Arm 1 features an LP P_1 and QWP W_1 between the BS and the convex lens L_1. In the other test arms, only an LP is placed in front of the convex lens. Correlation calculation of the intensity signal is measured by the four detectors, and the speckle pattern. Distributions of the Stokes parameters can be obtained based on the ghost imaging. The Stokes parameters carry the polarization and the intensity information of the reflected light. Normalized Stokes parameters can be calculated using measured results, and a polarization image can be obtained using the calculated normalized Stokes parameters.

Suppose the polarization state of the laser source in the experimental setup is known. Stokes parameter *S* describes the polarization state of the light, and can be expressed as

$$S = \begin{bmatrix} I \\ Q \\ U \\ V \end{bmatrix} = \begin{bmatrix} I_0 \\ I_x - I_y \\ I_{\pi/4} - I_{-\pi/4} \\ I_R - I_L \end{bmatrix}, \tag{1}$$

where I_0 represents total light intensity, I_x represents the horizontal polarization, I_y represents the vertical polarization, $I_{\pi/4}$ represents the linear π/4 polarization, $I_{-\pi/4}$ represents the linear -π/4 polarization, I_R represents the right circle polarization and I_L represents the left circle polarization. *DOP* can be defined as

$$DOP = \frac{\sqrt{Q^2 + U^2 + V^2}}{I} \tag{2}$$

The polarization state changes when light is reflected from the target, in accordance with the polarization state of the light illuminated on the target. The polarization state of reflection light $\mathbf{S}'$ is

$$\mathbf{S}' = \begin{bmatrix} I' \\ Q' \\ U' \\ V' \end{bmatrix} = \begin{bmatrix} m_{11} & m_{12} & m_{13} & m_{14} \\ m_{21} & m_{22} & m_{23} & m_{24} \\ m_{31} & m_{32} & m_{33} & m_{34} \\ m_{41} & m_{42} & m_{43} & m_{44} \end{bmatrix} \begin{bmatrix} I \\ Q \\ U \\ V \end{bmatrix} = \mathbf{MS}, \tag{3}$$

where matrix **M** is the Mueller matrix, which describes the influence of the target surface on the polarization state of the illuminating light.

As mentioned above, the Stokes parameters of the light reflected from the target (I', Q', U', V') are measured. The intensity signals i_1, i_2, i_3 and i_4 measured by the four independent detectors B_1, B_2, B_3 and B_4 calculate Stokes parameter $\mathbf{S}'$. The relationship between signal intensity and Stokes parameter is expressed as

$$\mathbf{I} = \begin{bmatrix} i_1 \\ i_2 \\ i_3 \\ i_4 \end{bmatrix} = \begin{bmatrix} a_{11} & a_{12} & a_{13} & a_{14} \\ a_{21} & a_{22} & a_{23} & a_{24} \\ a_{31} & a_{32} & a_{33} & a_{34} \\ a_{41} & a_{42} & a_{43} & a_{44} \end{bmatrix} \begin{bmatrix} I' \\ Q' \\ U' \\ V' \end{bmatrix} = \mathbf{A} \cdot \mathbf{S}', \tag{4}$$

where **I** is the intensity matrix of the four detectors and **A** is the matrix of the polarization detection system matrix.

As long as the polarization detection matrix is known and the determinant of matrix **A** does not equal 0, then $\mathbf{S}'$ can be derived according to

$$\mathbf{S}' = \mathbf{A}^{-1}\mathbf{I} \tag{5}$$

To guarantee that the determinant of matrix **A** is a nonzero number, the four test arms in the polarization detection system must be uncorrelated. When the determinant of matrix **A** is a nonzero number, matrix $\mathbf{A}^{-1}$ can be described as

$$\mathbf{A}^{-1} = \begin{bmatrix} a_{11}' & a_{12}' & a_{13}' & a_{14}' \\ a_{21}' & a_{22}' & a_{23}' & a_{24}' \\ a_{31}' & a_{32}' & a_{33}' & a_{34}' \\ a_{41}' & a_{42}' & a_{43}' & a_{44}' \end{bmatrix}. \tag{6}$$

According to Equation (5) and Equation (6), the following can be derived:

$$\mathbf{S}' = \begin{bmatrix} I' \\ Q' \\ U' \\ V' \end{bmatrix} = \begin{bmatrix} a_{11}{}' i_1 + a_{12}{}' i_2 + a_{13}{}' i_3 + a_{14}{}' i_4 \\ a_{21}{}' i_1 + a_{22}{}' i_2 + a_{23}{}' i_3 + a_{24}{}' i_4 \\ a_{31}{}' i_1 + a_{32}{}' i_2 + a_{33}{}' i_3 + a_{34}{}' i_4 \\ a_{41}{}' i_1 + a_{42}{}' i_2 + a_{43}{}' i_3 + a_{44}{}' i_4 \end{bmatrix}. \tag{7}$$

In GI the intensity image can be obtained by correlation calculation between the speckle pattern modulated by the SLM and the intensity signal measured by the bucket detector. Ghost imaging is expressed as [6–9]

$$G(x) = \frac{1}{N}\sum_{j=1}^{N} I_B{}^{(j)} I^{(j)}(x) - \frac{1}{N}\sum_{j=1}^{N} I_B{}^{(j)} \cdot \frac{1}{N}\sum_{j=1}^{N} I^{(j)}(x), \tag{8}$$

where N represents the total number of measurements is the signal intensity of the non-spatial detector in the j^{th} experiment, and $I^{(j)}(x)$ is the speckle pattern in the j^{th} measurement.

In CPGI system, the polarization state is described by Stokes parameters $[Q\ U\ V]^T$. For the normalized Stokes parameters the values Q, U, V are all in the interval of $\left[-1, \quad 1\right]$ and the value of I is 1. In order to describe the polarization state distribution intuitively, the intervals of three Stokes parameters $[Q\ U\ V]^T$ are all divided into 256 grey levels; that is, [0,255]. The mapped Stokes parameters are expressed with $[R\ G\ B]^T$, which follow the relationship

$$\begin{cases} R = \dfrac{255}{2}(Q+1) \\ G = \dfrac{255}{2}(U+1). \\ B = \dfrac{255}{2}(V+1) \end{cases} \tag{9}$$

he mapped Stokes parameter $[R\ G\ B]^T$ is defined as polarized chromatic value (PCV); thus, the distribution of PCV expresses the polarization state distribution of the target. Basically, the PCV distribution image is the target's polarization image.

By submitting Equation (9) into Equation (2), the relationship between polarization intensity and PCV is expressed as

$$DOP = \sqrt{\left(\frac{2R}{255} - 1\right)^2 + \left(\frac{2G}{255} - 1\right)^2 + \left(\frac{2B}{255} - 1\right)^2}. \tag{10}$$

According to Equation (6), in the j^{th} measurement, the components of Q, U and V are

$$\begin{cases} I_Q^{(j)} = a_{21}{}' i_1^{(j)} + a_{22}{}' i_2^{(j)} + a_{23}{}' i_3^{(j)} + a_{24}{}' i_4^{(j)} \\ I_U^{(j)} = a_{31}{}' i_1^{(j)} + a_{32}{}' i_2^{(j)} + a_{33}{}' i_3^{(j)} + a_{34}{}' i_4^{(j)} \\ I_V^{(j)} = a_{41}{}' i_1^{(j)} + a_{42}{}' i_2^{(j)} + a_{43}{}' i_3^{(j)} + a_{44}{}' i_4^{(j)} \end{cases}, \tag{11}$$

where $i_k^{(i)}$ is the signal intensity measured by non-spatial bucket detector B_k in the j^{th} measurement and k=1,2,3,4. In the polarization ghost imaging system, $I_B^{(j)}$ of Equation (7) is obtained by

$$I_B{}^{(j)} = I_P{}^{(j)}, P = Q, U, V. \tag{12}$$

The PCV distribution of the target can be achieved through Equation (8) and Equation (11). The proposed system can also be used to measure the intensity image of a target. Suppose that

$$I_I{}^{(j)} = a_{11}{}' i_1{}^{(j)} + a_{12}{}' i_2{}^{(j)} + a_{13}{}' i_3{}^{(j)} + a_{14}{}' i_4{}^{(j)}. \tag{13}$$

When $I_B^{(j)} = I_I^{(j)}$, the intensity image can be calculated by plugging Equation (13) into Equation (7).

3 COMPUTATIONAL EXPERIMENTATION WITH COLOUR FUSION POLARIZATION GHOST IMAGING (CPGI)

This section details our computational experiment, conducted in order to validate the theoretical analysis and compare the differences between both the polarized image and intensity image gathered by GI. In the simulation, an English character ‘H’ is selected as the target (see Figure 2).

Area A is wood, Area B is steel, Area C is stone. Area D, the background, is leaf cover. Equations (14)-(17) are the Mueller matrices of the different materials [21, 22]:

$$\mathbf{M}_{wood} = \begin{bmatrix} 1 & 0.01 & 0.03 & -0.02 \\ -0.01 & 0.20 & 0.03 & -0.03 \\ 0.01 & 0.06 & 0.23 & 0.02 \\ -0.01 & -0.01 & -0.04 & 0.16 \end{bmatrix}, \tag{14}$$

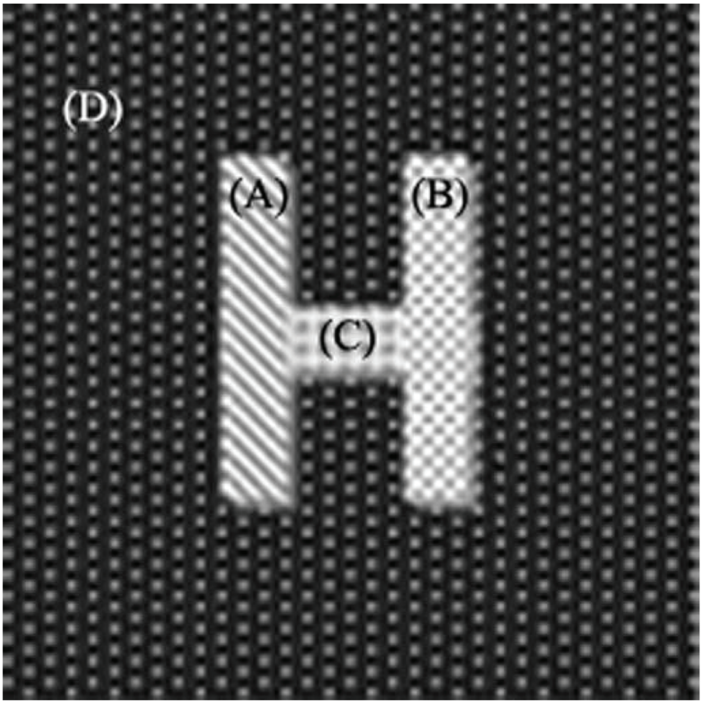

FIGURE 2
An English character ‘H’ is divided into four areas, all made of different materials.

$$\mathbf{M}_{steel} = \begin{bmatrix} 1 & 0.01 & 0.01 & 0.01 \\ -0.02 & 0.97 & -0.03 & 0.02 \\ -0.01 & 0.05 & 0.98 & 0.01 \\ 0.01 & 0.02 & 0.01 & 0.99 \end{bmatrix}, \tag{15}$$

$$\mathbf{M}_{stone} = \begin{bmatrix} 1 & -0.01 & 0.01 & 0.02 \\ 0.01 & 0.39 & 0.01 & -0.01 \\ -0.02 & 0.02 & 0.38 & 0.01 \\ 0.01 & 0.01 & -0.02 & 0.35 \end{bmatrix}, \tag{16}$$

$$\mathbf{M}_{leaf} = \begin{bmatrix} 1 & 0.0227 & -0.0031 & -0.0028 \\ 0.0077 & 0.2066 & -0.0038 & -0.0096 \\ 0.024 & 0.045 & 0.235 & -0.032 \\ 0.041 & 0.024 & 0.017 & 0.538 \end{bmatrix}. \tag{17}$$

The experiment takes place under ideal circumstances: it is assumed that there is no shot noise in the detector and no atmosphere turbulence in the test arm. In addition, the reflection coefficients of all areas shown in Figure 2 are the same. During the computational experiment, the polarization state of the illuminating light is horizontal polarization, because the SLM is sensitive to horizontal polarization light. The Stokes parameter of the illuminating light is $[1\ 1\ 0\ 0]^T$. System matrix **A** of the polarization detection system is measured by the Equator-Poles method [23]:

$$\mathbf{A}=\begin{bmatrix}0.922 & 0.908 & 0.081 & 0.014\\ 0.945 & 0.015 & -0.928 & 0.144\\ 1.078 & -1.069 & 0.005 & 0.017\\ 0.979 & -0.012 & -0.491 & 0.831\end{bmatrix}. \tag{18}$$

The determinant of the polarization detection system matrix **A** is calculated as: det(**A**)=-1.42; the polarization detection system matrix is a non-singular matrix, and inverse matrix $\mathbf{A}^{-1}$ exists.

In the calculation experiment, target polarization images are obtained with either 10000 measurements or 20000 measurements. Results are shown in Figure 3. Figures 3(a) to (c) are the RGB component distributions of the PCV and Figures 3(d) to (f) are the reconstructed images. The left side of each figure is the result with 10000 measurements and the right side is the result with 20000 measurements. The RGB component distributions of the PCV correspond to the distribution of Stokes parameters (Q, U and V). Figure 3(d) is the polarization image of the target and Figure 3(e) is the intensity image obtained by the GI. Target polarization intensity distributions can be obtained using the R, G and B component distributions according to Equation (2). Target polarization intensity distributions obtained in our experiment are shown in Figure 3(f).

As shown in the target polarization image in Figure 3(d), different materials correspond to different colours. The PCV of Area A (wood) is (98, 132, 66), resulting in a dark olive green. The PCV of Area B (steel) is (126, 93, 112), resulting in a dark plum colour. The PCV of Area C (stone) is (200, 130, 127), resulting in a dark pink colour. The PCV of the leaf is (108, 168, 175), which resulted in slate grey.

Figure 3(e) shows the target intensity image built with CGI, which is blank because it is assumed that the reflection coefficients of the target and background are the same. In Figure 3(d), different areas (A, B, C, and D) of the target correspond to different colours. The target is much more easily distinguished from the background in Figure 3(d) than Figure 3(e).

Target polarization intensity distributions can also be utilized to distinguish different target areas, as shown in Figure 3(f). DOP of each area (A, B, C and D) are calculated using

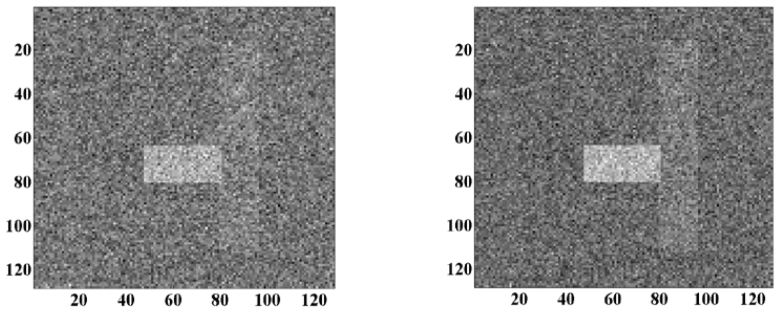
20
40
60
80
100
120
20 40 60 80 100 120

(a)

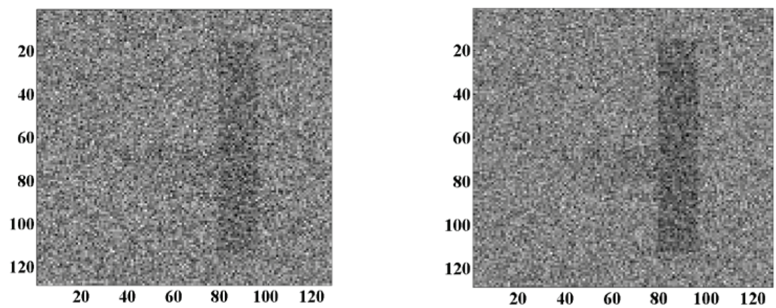
20
40
60
80
100
120
20 40 60 80 100 120

(b)

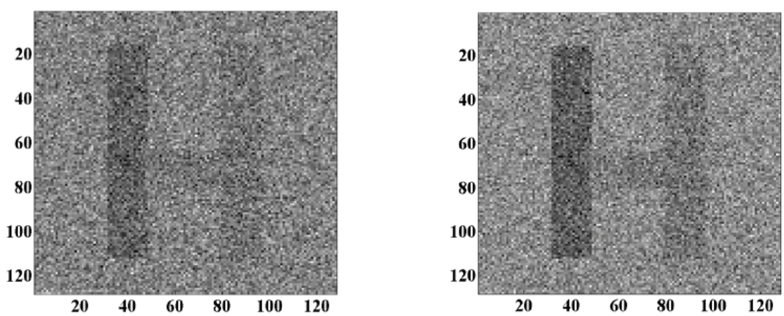
20
40
60
80
100
120
20 40 60 80 100 120

(c)

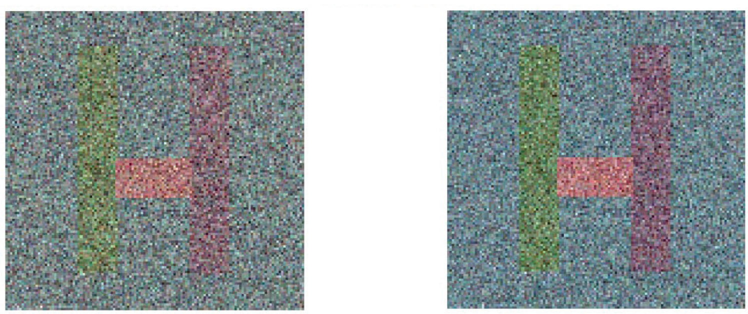

(d)

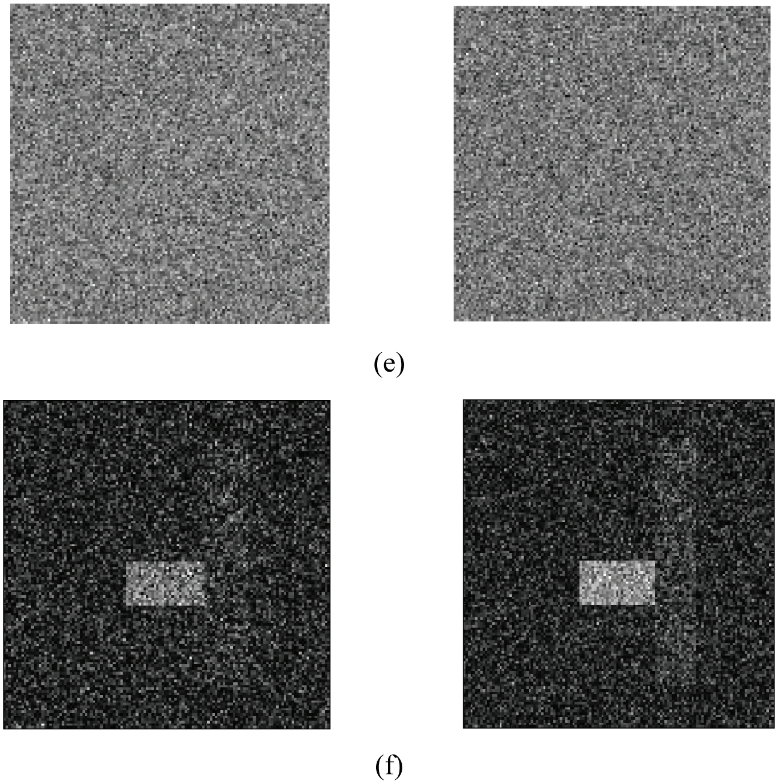

FIGURE 3
Simulation results with 10000 (left) and 20000 (right) measurements for (a) R component PCV distributions, (b) G component PCV distributions, (c) B component PCV distributions, (d) polarization images based on PCV, (e) target intensity images and (f) target polarization intensity distributions.

$$\begin{cases} DOP_A = \dfrac{1}{n_A}\sum\limits_{i}^{n_A} PI_i \\ DOP_B = \dfrac{1}{n_B}\sum\limits_{i}^{n_B} PI_i \\ DOP_C = \dfrac{1}{n_C}\sum\limits_{i}^{n_C} PI_i \\ DOP_D = \dfrac{1}{n_D}\sum\limits_{i}^{n_D} PI_i \end{cases}, \tag{19}$$

where $DOP_K(K=\mathrm{A},B,C,D)$ represents the polarization intensities of different areas, $n_K(K=\mathrm{A},B,C,D)$ represents the total number of pixels in different areas

TABLE 1
Polarization intensities of the four areas.

Material	**DOP**
Wood (Area A)	0.0386
Stone (Area B)	0.1686
Steel (Area C)	0.8606
Leaf (Area D)	0.0515

and DOP_i represents the polarization intensity of pixel i. Table 1 shows the polarization intensities of all four areas calculated according to Equation (19). Polarization intensity of the Area A is 0.0386 and 0.0515 for Area D – almost identical values. To this effect, Area A and Area D are difficult to see in Figure 3(f). The greater difference in PCV values for the two areas shown in Figure 3(d) make the corresponding colours much more different. This phenomenon suggests that PCV depicts target areas more effectively than polarization intensity.

The quality of reconstructed image with 20000 measurements is better than the image built with 10000 measurements, as shown in Figure 3. PCV measurement error under changing measurements is also calculated as shown in Figure 4. The error between measured results and results expected based on Mueller matrices is between 5 and 20%, and error decreases with increased number of measurements.

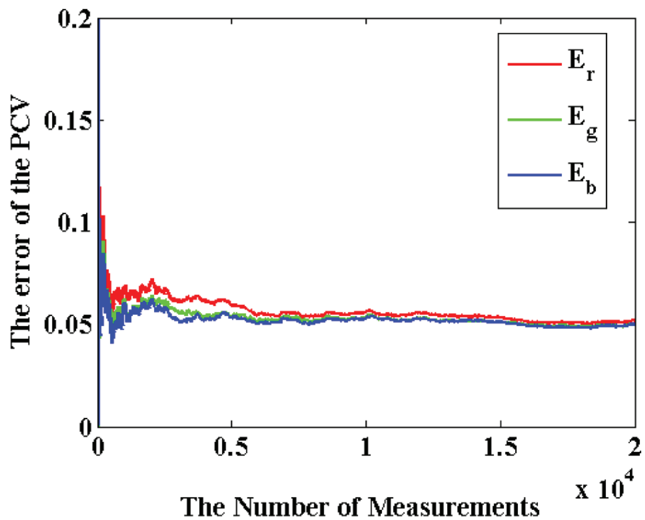

FIGURE 4
Graph showing PCV errors change with increasing number of measurements.

In the polarization image based on ghost imaging, errors in the RGB component distributions of the PCV are caused by noise of each RGB component distributions. According to ghost imaging theory, signal to noise ratio (SNR) is expressed as [24–26]

$$SNR = G(x)/\Delta G(x) \tag{20}$$

If measurements increase N times, SNR increases $\sqrt{N}$ times. As shown in Figure 4, it is reasonable to assume that increasing the number of measurements will decrease the error between measured results and results expected from Mueller matrices. The reduced decline rate of the error will decrease with the increasing measurement number as well.

In this computational experiment, the RGB components of the PCV values are obtained by 20000 measurements and the error of the PCV values is close to 5%. Therefore, the measured results agree with the results expected from these Mueller matrices.

4 CONCLUSIONS

This paper proposes a novel polarization ghost imaging system based on Stokes parameters. colour fusion polarization ghost imaging (CPGI) is proposed to allow measurement of the Stokes parameters distribution of the light reflected from a target. Polarized chromatic value (PCV) is defined in this study to describe the Stokes parameters distribution of reflected light in a pseudo-colour way; PCV distribution forms the polarization image. Computational experiments further validated the polarization ghost imaging system, using an H-shaped simulated target comprised of different materials (wood, stone, and steel) and a background (leaf cover). Experiment results showed that the proposed CPGI system successfully distinguished the target from the background, as the reflection coefficients of the target and background were equivalent. And CPGI system has a better capacity than polarization ghost imaging (PGI) system. The approach in this paper extends the application of the ghost imaging beyond measuring intensity range and image range, allowing additional information regarding targets to be gathered effectively.

REFERENCES

[1] Valencia A., Scarcelli G., D'Angelo M. and Shih Y. Two-photon imaging with thermal light. *Physical Review Letters* **94**(6) (2005), 063601.

[2] Basano L. and Ottonello P. Experiment in lensless ghost imaging with thermal light. *Applied Physics Letters* **89**(9) (2006), 091109.

[3] Gatti A., Bache M., Magatti D., Brambilla E., Ferri F. and Lugiato L.A. Coherent imaging with pseudo-thermal incoherent light. *Journal of Modern Optics* **53**(5–6) (2006), 739–760.

[4] Ferri F., Magatti D., Sala V.G. and Gatti A. Longitudinal coherence in thermal ghost imaging. *Applied Physics Letters* **92**(26) (2008), 261109.

[5] Ferri F., Magatti D., Gatti A., Bache M., Brambilla E. and Lugiato L.A. High-resolution ghost image and ghost diffraction experiments with thermal light *Physical Review Letters* **94**(18) (2005), 183602.

[6] Shapiro J.H. Computational ghost imaging. *Physical Review A* **78**(6) (2008), 061802.

[7] Bromberg Y., Katz O. and Silberberg Y. Ghost imaging with a single detector. *Physical Review A* **79**(5) (2009), 053840.

[8] Erkmen B.I. and Shapiro J.H. Ghost imaging: from quantum to classical to computational. *Advances in Optics and Photonics* **2**(4) (2010), 405–450.

[9] Katz O., Bromberg Y. and Silberberg Y. Compressive ghost imaging. *Applied Physics Letters* **95**(13) (2009), 131110.

[10] Gong W. and Han S. Multiple-input ghost imaging *via* sparsity constraints. *Journal of the Optical Society of America A: Optics, Image Science and Vision* **29**(8) (2012), 1571–1579.

[11] Zhao C., Gong W., Chen M., Li E., Wang H., Xu W. and Han S. Ghost imaging lidar via sparsity constraints. *Applied Physics Letters* **101**(14) (2012), 141123.

[12] Gong W. and Han S. Phase-retrieval ghost imaging of complex-valued objects. *Physical Review A* **82**(2) (2010), 023828.

[13] Tian N., Guo Q., Wang A., Xu D. and Fu L. Fluorescence ghost imaging with pseudothermal light. *Optics Letters* **36**(16) (2011), 3302–3304.

[14] Tyler G.A. and Boyd R.W. Influence of atmospheric turbulence on the propagation of quantum states of light carrying orbital angular momentum. *Optics Letters* **34**(2) (2009), 142–144.

[15] Edgar M., Sun B., Bowman R., Welsh S. and Padgett M.J. 3D Computational Ghost Imaging. *Emerging Technologies in Security and Defence; and Quantum Security II; and Unmanned Sensor Systems X.* 23 September 2013, Dresden, Germany. **8899**, pp. 889902–1–6

[16] Cao D., Xu B., Zhang S. and Wang K. Color Ghost Imaging with Pseudo-White-Thermal Light. *Chinese Physics Letters* **32**(11) (2015), 114208.

[17] Zhu Y., Shi J., Li H. and Zeng G. Three-dimensional ghost imaging based on periodic diffraction correlation imaging. *Chinese Optics Letters* **12**(7) (2014), 071101.

[18] Shi D., Hu S. and Wang Y. Polarimetric ghost imaging. *Optics Letters* **39**(5) (2014), 1231–1234.

[19] Zhu Y., Shi J. and Yang Y. Polarization difference ghost imaging. *Applied Optics* **54**(6) (2015), 1279–1284.

[20] Shi D., Wang F. and Jian H. Compressed polarimetric ghost imaging of different material's reflective objects. *Optical Review* **22**(6), (2015), 882–887.

[21] Breugnot S. and Clémenceau P. Modeling and performances of a Polarization Active Imager at λ=806. *Optical Engineering* **39**(10) (2000), 2681–2688.

[22] Collet C., Zallat J. and Takakura Y. Clustering of Mueller matrix images for skeletonized structure detection. *Optics Express* **12**(7) (2004), 1271–1280.

[23] Azzam R.M.A. and Lopez A.G. Accurate calibration of the four-detector photopolarimeter with imperfect polarizing optical elements. *Journal of the Optical Society of America A: Optics, Image Science and Vision* **6**(10) (1989), 1513–1521.

[24] Cheng J., Han S. and Yan Y. Resolution and noise in ghost imaging with classical thermal light. *Chinese Physics* **15**(9) (2006), 2002–2006.

[25] Bai Y, Yang K, Yang W and Yu X. Noise analysis in correlated imaging, quantum and classical. *Optik* **122**(20) (2011), 1791–1794.

[26] Erkmen B.I. and Shapiro J.H. Signal-to-noise ratio of Gaussian-state ghost imaging. *Physical Review A* **79**(2) (2009), 023833.